Control System Design for Double Gimbaled Wheels

J.J. Kalley Jr.*
TRW Systems, Redondo Beach, Calif.

Double gimbaled momentum wheel servo design is greatly influenced by factors which include gimbal/rotor flexibility, wheel nutation, rotor inertia cross product, wheel induced vibrations and gimbal friction. How to contend realistically with these effects rests on the mathematical models and design procedures which are utilized, and the sensitivity of the specific control concept to the gimbal and rotor disturbances. In this respect, a control method known as precession control has proven useful. Performance data shows this control technique to have a very precise pointing capability while virtually immune to major electronics and mechanical disturbance factors.

Nomenclature

B, B_o, B_i = gimbal damping
d = spin bearing separation
H = rotor momentum
I_p, I_c = rotor polar/cross product inertia
I_o, I_i = gimbal/rotor outer inertia
J_w = rotor transverse inertia
K = rotor stiffness
K_o, K_i = precession control loop gain
K_p, K_{po}, K_{pi} = direct control position gain
K_r, K_{ri}, K_{ro} = direct control rate gain
p = P-plane operator
R = ratio of outer to polar inertia
s = Laplace operator
T_d = rotor disturbance torque
w_{go}, w_{gi} = gimbal resonance frequencies
w_s = rotor spin speed
w_τ = rate filter corner frequency
X_ϵ = spin bearing runout displacement
Ω = nutation frequency
θ_i = inner gimbal motion
$\Delta\theta_i$ = inner gimbal offset
$\dot{\theta}_{iL}$ = maximum gimbal slew rate
θ_o = outer gimbal motion
τ = rate filter time constant

Model Parameters

J_{wi}, J_{wo} = transverse rotor inertia
I_{i2} = inner gimbal trunnion and drive shaft about inner axis inertia
I_{il} = inner gimbal ring about inner axis inertia
I_{o2} = outer gimbal trunnion and drive shaft about outer axis inertia
I_{ol} = outer gimbal ring and inner gimbal ring about outer axis inertia
K_{i2} = inner gimbal trunnion, drive shaft, and gimbal ring stiffness about inner axis
K_{il} = transverse rotor web, rotor bearing, and rotor shaft stiffness about inner axis
K_{o2} = outer gimbal trunnion, drive shaft, and gimbal ring stiffness about outer axis
K_{ol} = inner gimbal shaft, inner ring and transverse rotor web, rotor bearing, and rotor shaft stiffness about outer axis
B_i, B_o = viscous friction of inner and outer gimbal
B_{il}, B_{i2} = inner gimbal structural damping
B_{ol}, B_{o2} = outer gimbal structural damping
τ_{mi}, τ_{m0} = inner and outer gimbal motor torque

Presented as Paper 74-895 at the AIAA Mechanics and Control of Flight Conference, Anaheim, California, August 5-9, 1974; submitted September 10, 1974; revision received March 3, 1975. This paper is based upon work under the sponsorship of the International Telecommunication Satellite Organization (INTESLSAT). Any views expressed are not necessarily those of INTELSAT.

Index category: Spacecraft Attitude Dynamics and Control.

*Member of the Technical Staff. Member AIAA.

Introduction

GIMBALED wheels, specifically double-gimbaled momentum wheels (DGMW), have a complex set of high-frequency resonance dynamics. These are the result of rotor and gimbal flexibility and the DGMW rotor nutation. A high-speed conical whirl of the rotor is noted (even for the ideal case of a rigid rotor and gimbal structure) in the same sense as the spin of the rotor. This motion is termed nutation, and its frequency for the ideal nonflexible DGMW is numerically, $\Omega = I_p w_s / (I_o I_i)^{1/2}$, where w_s is the rotor spin speed, I_p is the rotor polar inertia, and I_o and I_i are the effective DGMW transverse inertias. By itself, the rotors' transverse inertias are roughly $I_o = I_i = I_p/2$, which results in $\Omega = 2w_s$. With the addition of the gimbal structure inertias, Ω can take on values which may approach or equal the spin speed. If this condition should exist, any spin-oriented disturbance such as dynamic unbalance in the rotor or bearing runout would cause large amplitudes of whirl and vibration for any spin speed.

Flexible structures alter the nutation frequency characteristics[1] to the extent that the ratio to the spin speed no longer remains constant, and, in addition, the flexibility complicates the dynamic mechanical design by producing more than one critical spin speed. Gimbal control is also affected by interactions with these high-frequency dynamics; specifically for the task of stabilizing the gimbals during rotor runup or rundown.

Other influences upon gimbal control design are the desire to: 1) process the spacecraft control gimbal commands and resolver readouts digitally to preserve accuracy; 2) stabilize the gimbals without tachometers so as to ease the mechanical integration problems; and 3) perform gimbal control in an available flight processor to afford a savings in analog components provided the computer capacity is not adversely affected.

Gimbal controls, specifically large-angle d.c. torquer drives, can be implemented by two distinct techniques; direct drive or precession control. The direct drive is a conventional rate plus position feedback approach which has a number of limitations due to the rate noise generated by gimbal vibrations and position quantization. The precession technique is well suited to a DGMW application provided the wheel is spinning. This control is implemented by cross-

strapping the gimbal angles in the sense that the outer gimbal drives the inner torquer and the reverse for the outer torquer. The principal advantages are that rate derivation is not required when the wheel is spinning, and the control is easily implemented if gimbal angles do not exceed 15-20°.

The primary purpose of this paper is to present a brief survey of the fundamental double-gimballed wheel dynamics, and to relate how disturbances impact the gimbal mechanical and control design. The control concepts contained in this paper are restricted to gimbal controls and do not include considerations of the interaction with rotor speed control. Analysis and bench test shows this to be a justifiable approximation due to the second-order nature of the coupling at small angles.

Illustrative examples are used which draw upon the experiences and data accumulated during the past several years with respect to the design and development of DGMW hardware systems. The most recent system is an engineering model of a 30 ft-lb-sec system for possible use in a fully stabilized synchronous communication satellite application.[2]

Gimbal and Rotor Flexibility Considerations

Free Gimbal Systems

The general concern when establishing proper gimbal suspension and rotor flexibility design goals is to assure, throughout the usable wheel speed range, that the wheel nutation frequency, the spin frequency, and the structure resonances are sufficiently separated. If this condition is not upheld, dynamic imbalance or bearing runout will cause large-amplitude wheel and gimbal vibrations.

Since the transmissibility of the rotor resonances can reach large factors, it is necessary to restrict the ratio of rotor speed (w_s) to nutation frequency (Ω) such that

$$w_s/\Omega<0.8 \quad \text{or} \quad w_s/\Omega>1.2 \tag{1}$$

To demonstrate the basic thrust of this condition, assume the case of an uncontrolled rigid gimbal and rotor system with the linearized dynamics

$$I_o\ddot{\theta}_o+H\dot{\theta}_i+B\dot{\theta}_o=T_d\cos w_s t$$

$$I_i\ddot{\theta}_i-H\dot{\theta}_o+B\dot{\theta}_i=T_d\sin w_s t \tag{2}$$

$$H=I_p w_s$$

where T_d represents a rotor fixed torque such as produced by a dynamic unbalance. The magnitude of the spin-speed component of the inner gimbal motion due to this torque is

$$\dot{\theta}_t=\frac{[T_d(B^2+(I_o+I_p)^2w_s^2)^{1/2}}{I_oI_i(\Omega^2-w_s^2)^2+B^2([I_o+I_i]/I_oI_i)^2\cdot w_s^2)^{1/2}} \tag{3}$$

The outer gimbal can be similarly described. Clearly, since I_o and I_i include gimbal suspension inertias as well as the rotor transverse inertia the ideal nutation frequency could assume a relatively wide range of values, including the critical value $\Omega=w_s$. The transmittance as a function of the ratio $R=I_o/I_p$ assuming $I_i=I_o/2$ and $B=0.015$ ft-lb-sec is shown in Fig. 1. The design constraint given in Eq. (1) clearly follows.

The results shown in Fig. 1 can be misleading because flexible structures are missing. A more complex structural model, such as that shown in Fig. 2, produces a nutation frequency which changes as a function of wheel speed, and has the added complications of the gimbal suspension dynamics. A design based upon this model can become involved. To reduce the complexity, a procedure can be used which separates the design into two parts. First, select rotor stiffness assuming rigid gimbals. Then, select gimbal stiffness which offer minimum interference with the rotor resonances.

The gimbal dynamics model, assuming structural/gimbal damping and gimbal compliance can be ignored, is

$$J_{w_i}\ddot{\theta}_i-H\dot{\theta}_0+K_{il}(\theta_i-\theta_{il})=T_{di}$$

$$J_{w_o}\ddot{\theta}_o+H\dot{\theta}_i+K_{ol}(\theta_o-\theta_{ol})=T_{do}$$

$$I_{il}\ddot{\theta}_{il}+K_{il}(\theta_{il}-\theta_i)=0$$

$$I_{ol}\ddot{\theta}_{ol}+K_{ol}(\theta_{ol}-\theta_o)=0 \tag{4}$$

The characteristic equation for Eq. (4) is of the form

$$CE=s^2(a_1s^6+a_2s^4+a_3s^2+a_4) \tag{5}$$

With the additional assumptions that the rotor transverse stiffness and inertias are nearly equal such that, $J_{wi}=J_{wo}=J_w$, and $K_{ol}=K_{il}=K$, the coefficients are

$$a_1=J_w^2I_{il}I_{ol}$$

$$a_2=J_wK[I_{ol}(J_w+I_{il})+I_{il}(J_w+I_{ol})]+H^2I_{il}I_{ol}$$

$$a_3=K^2(I_{il}+J_w)(I_{ol}+J_w)+H^2K(I_{ol}+I_{il})$$

$$a_4=H^2K^2 \tag{6}$$

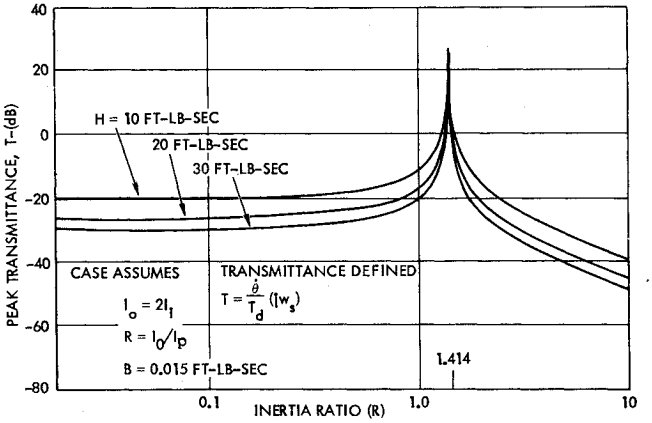

Fig. 1 Double-gimbaled wheel transmittance for rotor fixed torque assuming rigid rotor and gimbals.

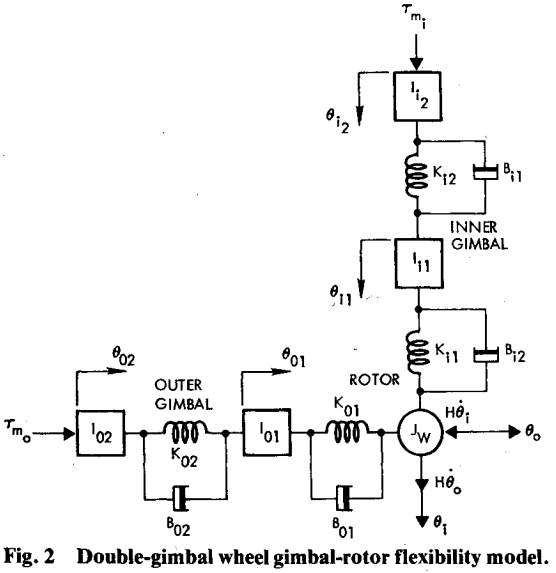

Fig. 2 Double-gimbal wheel gimbal-rotor flexibility model.

Substituting for the Laplace operator such that:

$$p=s^2$$

and regrouping Eq. (5) into coefficients with and without the term H^2 yields the form

$$CE=p[A(p)H^2+B(p)] \tag{7}$$

where

$$A(p)=p^2I_{il}I_{ol}+pK(I_{ol}+I_{il})+K^2$$

and

$$B(p)=p(p^2J_w^2I_{il}I_{ol}+p(J_wK(I_{ol}(J_w+I_{il})$$

$$+I_{il}(J_w+I_{ol}))+K^2(I_{il}+J_w)(I_{ol}+J_w))$$

The nature of this function can be investigated by placing Eq. (7) into the root locus form:

$$CE=B(p)p(1+G(p)), \quad G(p)=H^2[A(p)/B(p)] \tag{8}$$

$A(p)$ has the form $(p+P_1)(p+P_2)$ where $P_1=K/I_{ol}$, $P_2=K/I_{il}$. These represent the transverse resonances at $H=0$. $B(p)$ has the form $(p+P_3)\cdot(p+P_4)\cdot(p+P_5)$ where

$$P_3=\frac{K(I_{il}+J_w)}{J_wI_{il}}, \quad P_4=\frac{K(I_{ol}+J_w)}{J_wI_{ol}}, \quad P_5=0$$

Typical gimbal design is such that $I_{il}\leq J_w\leq I_{ol}$. With these relative magnitudes the conditions exist that

$$P_1\leqslant P_2\leqslant P_3 \text{ and } P_1\leqslant P_4\leqslant P_3 \tag{9}$$

The root P_4 may or may not be greater than P_2. Figure 3 shows the loci of the roots of $1+G(P)$ as H^2 increases. The $H=0$ root at the origin moves toward the zero at P_1, P_4 moves toward the zero P_2 and P_3 increases toward zero at infinity. Thus, for sufficiently large H, the system resonances approach the zero speed resonances.

Since the roots move as a function of momentum, a logical design procedure is to insure no critical wheel speeds will exist by setting

$$P_3\geq P_1>w_s^2 \quad \text{and} \quad P_4>w_s^2 \tag{10}$$

A low-frequency root P_Ω, replaces the nutation frequency of the rigid model, and to prevent a critical condition it is restricted to the condition $P_\Omega<w_s^2$. A conservative estimate of P_Ω can be gained by forming the ratio of the last two terms of the CE given in Eq. (5); e.g.,

$$P_\Omega=\frac{a_4}{a_3}=\frac{H^2K^2}{KH^2(I_{ol}+I_{il})+K^2(I_{il}+J_w)(I_{ol}+J_w)}<w_s^2 \tag{11}$$

This estimate of P_Ω is found[1] to be less than the true value for all values of H.

Conditions (10) and (11) form the basic design goals; from these relationships, a selection is made of the maximum rotor speed, rotor momentum, and rotor shaft stiffness. The degree to which the inequalities are met depends somewhat on the transmittibility of the structure to spin oriented disturbances.

As an example, the inertias of a recent 30-ft-lb-sec wheel and the earlier disturbance model, yield a transmittance (Fig. 4) as a function of wheel speed and rotor stiffness which has a gain of 30 db at the rotor resonance. This implies that the maximum wheel speed should, in general, not lie closer than $\pm 20\%$ of the gimbal resonance; however, in the case of rotor disturbances, the wheel speed may pass through the resonance without causing harmful effects.

Gimbal Stiffness Effects

As in the case of rotor stiffness, the design goal is to insure the gimbal resonances are above the maximum rotor speed or at least of no consequence when the rotor speed passes through them. The gimbal resonance frequencies can be approximated by the simple expressions:

$$w_{gi}=(K_{i2}/I_{il})^{1/2}, \qquad w_{go}=(K_{02}/I_{0l})^{1/2} \tag{12}$$

In most cases, the design goal is to select $w_{gi}>w_s$ and $w_{go}>w_s$.

Gimbal Disturbances

Two major gimbal disturbances exist in the form of rotor dynamic unbalance and spin bearing runout. Dynamic unbalance in the form of rotor cross-product of inertia (I_c) can be reduced to a disturbance torque fixed to the rotor with the magnitude:

$$T_d=I_cw_s^2 \tag{13}$$

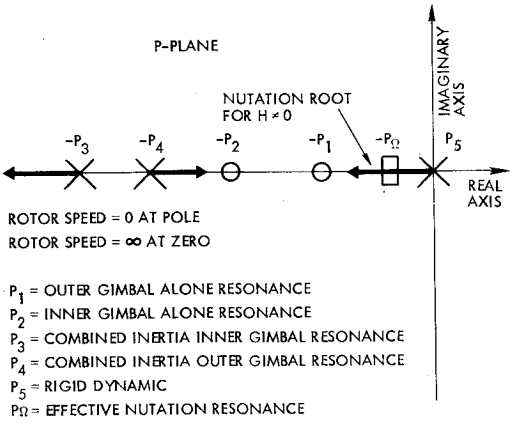

Fig. 3 Rotor flexibility P-plane root motion as a function of rotor speed.

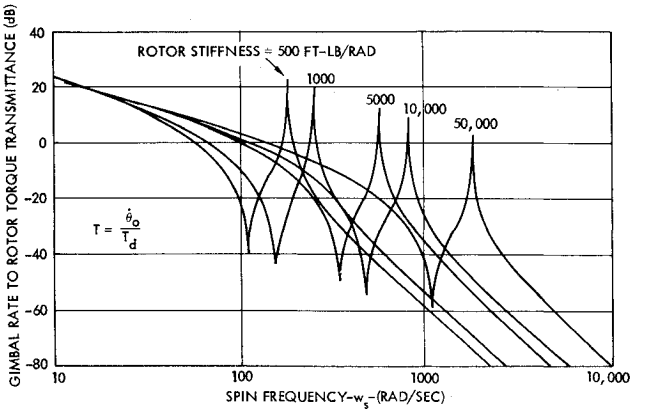

Fig. 4 Rotor torque transmittance to gimbal rate assuming rigid gimbals.

The effect of bearing runout can be obtained by modeling the disturbance as:

$$T_d = K\frac{X_\epsilon}{2d} \tag{14}$$

where X_ϵ is the bearing eccentricity and d is the distance between bearings. Nominal values are:

$$X_\epsilon = 10^{-5}\text{in.} \quad d = 4\text{in.} \tag{15}$$

A summary of these two effects upon gimbal rate is given in Table 1. The combined results of these two disturbances will produce an estimated gimbal rate dither at spin speed having peak values in the neighborhood of 0.5-1.0 deg/sec. The ultimate nature of the given disturbance varies from device to device, however, typical waveforms appear in Fig. 5. The beating noted in the figure is between the nutation and spin frequencies. The peaks can be seen to vary between 0.5-1.0 deg/sec.

DGMW Model Parameters

A number of tests on DGMW hardware were made to gather sufficient data to construct a mathematical model which could be used in the control system design and analysis. The model selected (shown in Fig. 2) assumes small angle and rate motion. See the Appendix for specific gimbal parameters.

Inertia and stiffness numbers were achieved through static tests. Gimbal viscous friction and structural damping coefficients were determined by noting the rate of decay and frequency (with the gimbal control off) of the gimbal nutation resonance at several values of steady-state rotor speed. When a comparison of this data (Fig. 6) was made to that obtained from the model of Fig. 2, a viscous friction of $B_o = B_i = 0.015$ ft-lb-sec was achieved.

Table 1 Estimate of motion produced by rotor disturbance torques

Source	Equivalent torque (ft-lb) $w_s = 400$ rad/sec	Gimbal rate (deg/sec)
Dynamic unbalance (0.05 oz-in^2)	0.11	0.62
Bearing runout (Stiffness $= 5 \times 10^4$ ft-lb/rad)	0.063	0.36
Total (max)	0.173	0.98

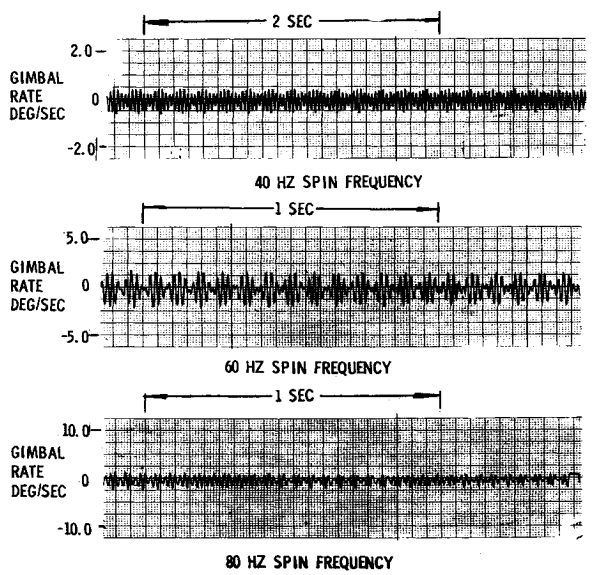

Fig. 5 Typical quiescent gimbal rate motion as a function of internal disturbance torques.

It is interesting to note that in the case of a rigid motor and gimbal, the nutation root at large H can be approximated as:

$$s^2 I_o I_i + Bs(I_o + I_i) + H^2 \tag{16}$$

If α is the real part of the nutation pole and ζ is the damping factor, then

$$\alpha = -\tfrac{1}{2}\frac{B(I_o+I_i)}{I_o I_i}, \quad \zeta = \frac{1}{2H}\frac{B(I_o+I_i)}{(I_o I_i)^{1/2}} \tag{17}$$

The nutation pole natural frequency is

$$\Omega^2 = H^2/I_o I_i \tag{18}$$

For the case $I_o = 0.1$ slug-ft^2, $I_i = 0.05$ slug-ft^2 and $H = 30$ fps, $\alpha = 0.2$, then $B = 0.0133$ ft-lb-sec. It is to be noted that the estimate shows α to be independent of the momentum H. In the more complex model (Fig. 2), the real part of the nutation pole becomes more negative as momentum increases.

The model structural damping terms were determined from the test data by noting the degree to which the loci bend to the left. In the case under study, these factors were determined to lie in the range of 0.002-0.005. It is also of interest to note that in comparing the nutation frequency of the simplified model [Eq. (2)] to the more complex model a marked difference appears at higher momentum. For example, at $H = 30$ ft-lb-sec, $\Omega = 425$ rad/sec, whereas from hardware and the more complex model $\Omega = 350$ rad/sec. The difference is due to the coupling of the compliance roots with the nutation pole.

Gimbal Friction

Bench test data for zero wheel speed indicated the existence of a constant gimbal torque, with respect to speed, of 0.006 ft-lb. This level dropped to 0.003 ft-lb when the wheel was spinning. No break-away torque was noted in the true sense of the word, since motion would be detected for very minute motor torques, particularly when the wheel was running. This freedom of motion is felt to be a result of "springy" bearings and the dithering effect of the spin induced vibrations. The predominant source of the constant torque was felt to be the torquer detent torque with some contribution due to the bearings, particularly at zero rotor speed. Decay motion of the nutation oscillation was observed to be exponential rather than linear with respect to time indicating that "coulomb" friction was minimal.

Gimbal Control Design

If relatively tight gimbal pointing is desired over the many possible flight environmental extremes, digital gimbal angle processing is considered the better approach. Gimbal freedom is normally less than $\pm 20°$ allowing the use of an 8-speed resolver. State-of-the-art 12-bit resolver-to-digital (R/D) converters yield an acceptable LSB of 0.011°. Command error signals can be developed digitally, digital-to-analog converted at desired scale levels and then used to drive a limited rotation d.c. torquer. The gimbals are, in general, driven as position servos; although in many spacecraft applications they could be driven as rate servos. The position approach has a more general application, since it is an inherently much more accurate means of control implementation.

Direct Control

The first control technique is a conventional configuration (Fig. 7), in which stabilization is achieved by electronically deriving rate or by installing a tachometer in each gimbal. The tachometer is more desirable due to the minimum phase lag

encountered; however the disadvantages of increased gimbal size and mechanical complexity make the derived rate approach more acceptable.

Rate can be developed by several electronic lead filters methods which include: 1) digital first differencing, 2) analog lead filtering of DAC signal, and 3) analog rate derivation from resolver converter logic signals. The primary design problem associated with lead filters are their response to noise. Two sources of noise exist in the form of discontinuities at each LSB change and the spin induced vibrations. These noise sources have little effect upon pointing accuracy due to the attenuation caused by the gimbal inertia, but to prevent overdriving the torquing device, low-pass filtering must be applied, however at the penalty of reducing the control bandwidth. In several large-momentum high-gimbal response applications constraints have surfaced which indicate that to obtain reasonable stability margins and to cope with the large transverse axis coupling torques, the position gain and rate gains must be relatively large. A single filter pole is allowed below the spin frequency, and if additional filtering is to be used it must produce less than 10° phase shift at the nutation frequency. The general result of these conditions is that little can be done to prevent noise from overdriving the gimbal torquers, unless performance degradation is accepted or oversized torquers are installed.

Precession Control Approach

As a means of bypassing the problems cited, a dual mode control can be designed which consists of a direct servo control for wheel speeds up to a certain value and a gimbal precession control[3] for higher speeds. The precession control (Fig. 8) does not require rate signals, thereby eliminating the rate derivation noise.

Precession Control Design

The high-speed rotor gimbal control design is based on the following: 1) low offset errors during gimbal unloading; 2) gimbal control bandwidth greater than the body control system bandwidth; and 3) suitable stability margins over operating speed range. The precession control can be designed roughly using the simple rigid wheel and gimbal model of Eq. (2).

The precession control laws can be approximated as

$$\tau_{m0} = -K_o(\theta_i - \theta_{ic}) \quad \tau_{mi} = +K_i(\theta_o - \theta_{oc}) \tag{19}$$

Combining and solving for θ_o and θ_i yields

$$\begin{bmatrix} \theta_o \\ \theta_i \end{bmatrix} = \frac{1}{D(s)} \begin{bmatrix} I_i s^2 + Bs & -(Hs + K_o) \\ Hs + K_i & I_o s^2 + Bs \end{bmatrix}$$

$$\times \begin{bmatrix} K_o \theta_{ic} \\ -K_i \theta_{oc} \end{bmatrix} \tag{20a}$$

$$D(s) = DET \begin{bmatrix} s^2 I_o + Bs & Hs + K_i \\ -(Hs + K_o) & I_i s^2 + Bs \end{bmatrix} \tag{20b}$$

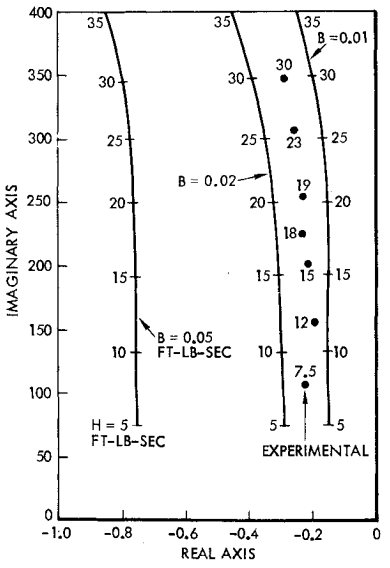

Fig. 6 Double gimbal wheel nutation pole loci (without gimbal control) for the Fig. 2 dynamics model.

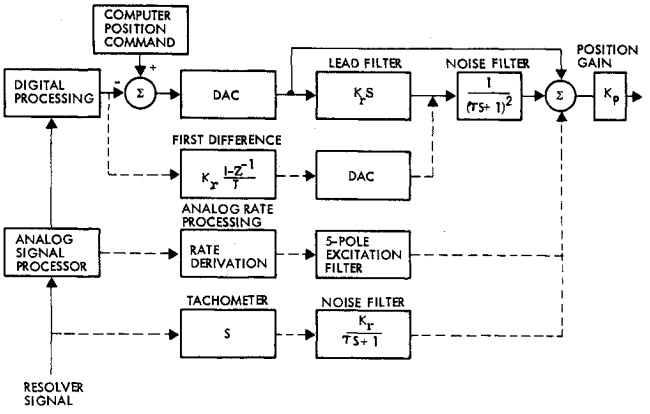

Fig. 7 Direct gimbal servo control with optional rate derivation concepts.

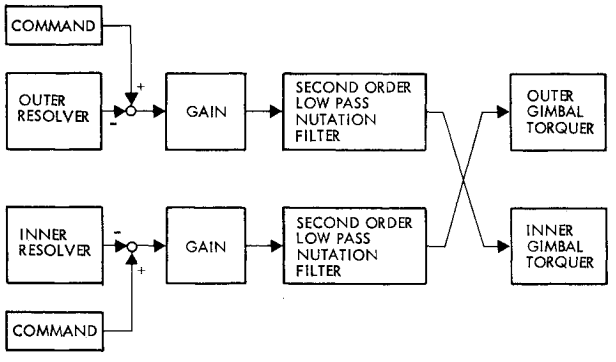

Fig. 8 Precession control technique.

The denominator term can be approximated for large H as

$$D(s) = (I_o I_s s^2 + B(I_o + I_i)s + H^2)$$

$$\times \left(s^2 + \frac{(K_o + K_i)}{H} s + \frac{K_o K_i}{H^2}\right) \tag{21}$$

Although this is often not accurate at low H, the low-frequency control root estimate proves to be good for determining the magnitude of the control gains for the normally high operating speed.

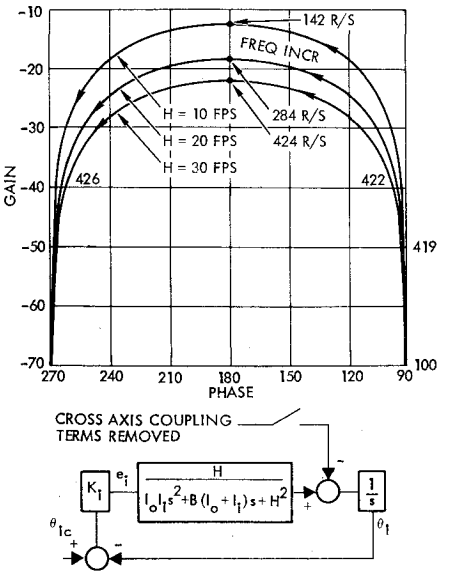

Fig. 9 Gain-phase plot of direct coupling transfer function.

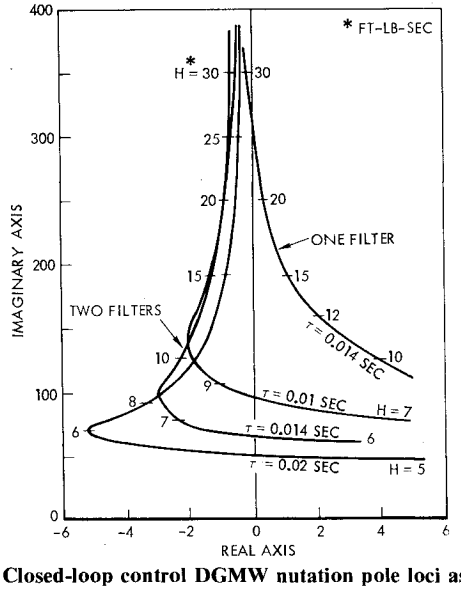

Fig. 10 Closed-loop control DGMW nutation pole loci as function of wheel speed and filter gains using a complex gimbal dynamics model.(Fig. 2).

When the unloading commands[2] are executed, the outer gimbal motor must produce the torque

$$\tau_{m0} = H\dot{\theta}_{iL} = K_o \Delta\theta_i \tag{22}$$

To minimize error during the slew maneuver

$$K_o = \geq H\dot{\theta}_{iL}/\Delta\theta_i \tag{23}$$

To have a suitable response during gimbal unloading and to have sufficient separation from the spacecraft controls, a bandwidth (ω_B) 10 times greater than the highest vehicle control frequency is acceptable. The control gains necessary to satisfy this are determined from the gimbal control root approximation; i.e.,

$$K_o K_i \geq H^2 \omega_B^2 \tag{24}$$

Precession Control Stability

A simple cross position feedback is not satisfactory in terms of loop stability over the operating wheel speed range of the control. This is true for even the simple dynamics model. For example, the parameters: $H=30$ ft-lb-sec, $I_o=0.1$ slug-ft^2, $I_i=0.05$ slug-ft^2, $B=0.015$ ft-lb-sec, and $K_o=K_i=150$ ft-lb/rad, yield the precise roots

$$D=(S-4.77\pm j424)\,(S+4.99\pm 0.0056) \tag{25}$$

which indicate the control roots are roughly those estimated, but the nutation pole is unstable.

The stability problem can be solved by phase stabilizing the nutation pole with filters in each feedback path. A measure of the problem at hand can be gained by examining the simple model [Eq. (20)] for the stability of the θ_i/τ_{mo} loop (such as shown in Fig. 9) without the coupling from the outer gimbal control. This form of analysis is not rigorous, but it does lead to a quick estimate of the filtering required.

A phase-gain plot of this function for the above gains appears in Fig. 9. It is clear from the plot that without filters the values for K_i must be small if stable control is to be maintained over a reasonable range of wheel speeds. Since this value would be too low to achieve the desired gimbal control bandwidth at $H=30$ ft-lb-sec, it is necessary to add low pass filters to the loop. The placement of the filter is a function of the control gain and the lowest operating wheel speed. Assume for the moment that $H=10$ ft-lb-sec is an acceptable lower limit, and $K_o=K_i=150$ ft-lb/rad, then stability of the simplified model can be achieved if 90° of phase shift can be gained before 90 rad/sec.

A two pole filter at 70 rad/sec would develop the required phase shift whereas a single pole filter would have to be placed at a much lower frequency and yield marginal results. To check this result in terms of the more complex dynamics, the nutation roots of a compliance-control model were extracted for filters with one and two poles at 70 rad/sec as shown in Fig. 10. Clearly, the simple model indicates the appropriate direction to take, since the two-pole design has produced a much greater speed range stability. An increase in the range of stable wheel speeds can be seen as the filter time constant is increased.(Fig. 10).

Typical Bench Performance

Step Response

The nominal design selected for the 30 ft-lb/sec DGMW has the filters set at 50 rad/sec and position gains of 150 ft-lb/rad in each axis.

The actual precession control performance for all stable speeds is very close to that estimated. For step commands which do not saturate the torquer the response is that of each axis decoupled and having a first order characteristic. When the step command saturates the torquer, the gimbal under command moves at a constant rate which is equal to gimbal torque limit divided by the momentum. The entrance and exit from the saturation condition, as shown in Fig. 11, is performed cleanly with no loss of control and minor cross-coupling into the other axis.

Nutation Stability

The low pass characteristic of the control loop implies the control does not stabilize the nutation resonance. This is a definite plus, since control energy is not expended at the relatively high nutation frequencies. However the question of adequate nutation stability must be answered. In this respect bench tests have shown sufficient gimbal damping exists to inhibit pronounced nutation oscillations. Under no circumstances was the control capable of exciting noticeable oscillations, and when these were excited by artificial means they quickly decayed (Fig. 12).

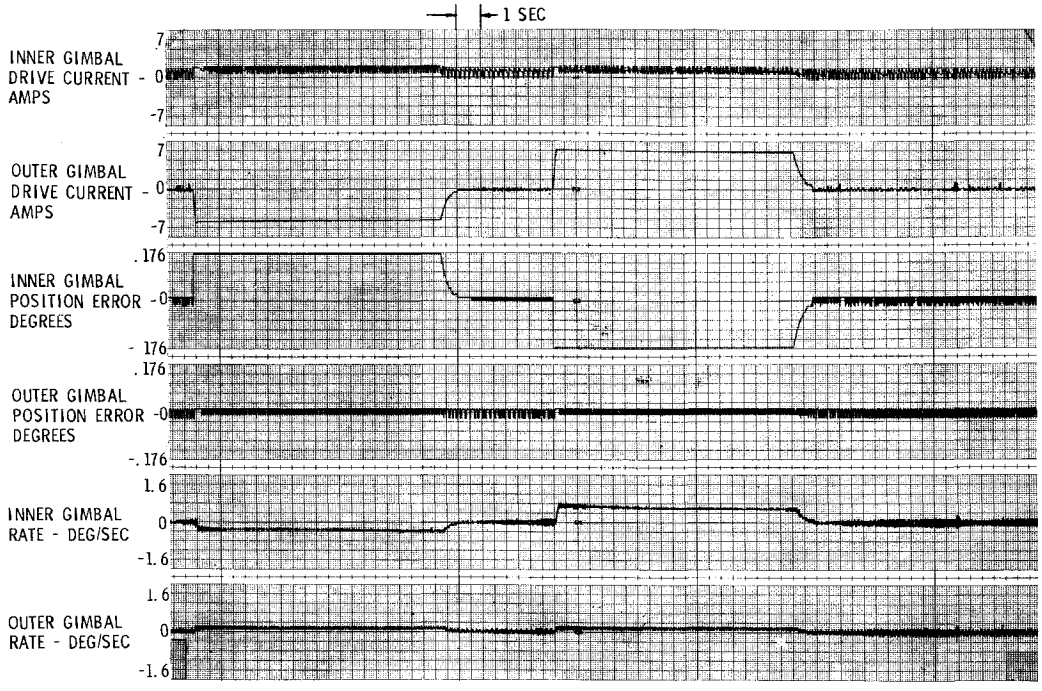

Fig. 11 Hardware bench test gimbal response at wheel speed of 80 Hz for inner gimbal command of 5.6° and a return to zero.

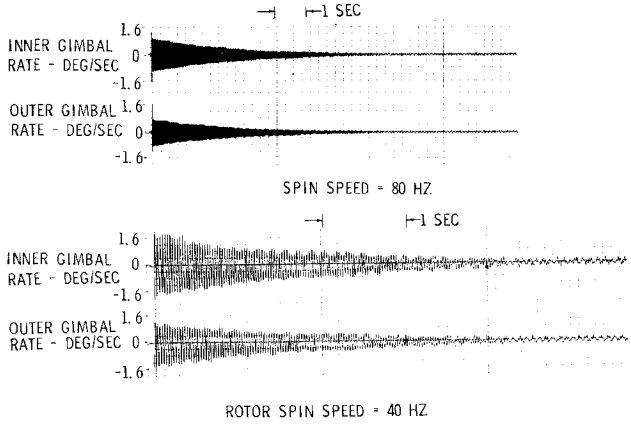

Fig. 12 Gimbal control response to an excited nutation oscillation for wheel speeds of 80 and 40 Hz.

Conclusions

The primary thrust of this paper has been one of illuminating a few of the more serious DGMW servo design problems. In this respect it is clear that appropriate rotor and gimbal stiffness values must be used, but the specific values depend greatly upon the wheel momentum, speed, and weight limitations. The approach of investigating transmittance rather than simply noting the relative position of the nutation and compliances roots, tends to be more realistic and can bring about a less conservative design resulting in a possible gimbal weight and size reduction. The method allows an estimate of gimbal noise to be obtained which is necessary when the control technique rests upon rate derivation.

The application of the control techniques to a recent 30 ft-lb-sec DGMW produced a system with electrical pointing accuracy within $\pm 0.02°$(LSB-0.011°) with virtually no coupling between axes during maximum slew rates of 0.25-0.5 deg/sec. For this specific case, substantially no excitations of the nutation or compliance resonances through control action were noted. When mechanically excited the nutation oscillations subsided in a reasonable time.

Appendix: Gimbal-Rotor Stiffness Parameters for a 30 ft-lb-sec DGMW

The inertia and stiffness constants were obtained from tests conducted at the Sperry Flight Systems Division, Phoenix, Ariz. The structural damping constants were selected to yield damping factors such that $\zeta < 0.005$ at the complience poles. The gimbal viscous damping factors were selected by matching model data against gimbal high-frequency test data. The inertia and stiffness parameters are computed or measured to be: $J_{wi} = J_{wo} = 0.0314$ slug-ft^2, $I_{i2} = 0.005$ slug-ft^2, $I_{il} = 0.0130$ slug-ft^2, $I_{o2} = 0.005$ slug-ft^2, and $I_{ol} = 0.0708$ slug-ft^2. The total inner axis inertia is $I_i = 0.044$ slug-ft^2 and the total outer axis inertia is $I_o = 0.1022$ slug-ft^2. $B_{il} = B_{i2} = B_{ol} = B_{o2} = 0.2$ ft-lb-sec, $K_{i2} = 1.53 \times 10^4$ ft-lb/rad, $K_{il} = 5.4 \times 10^4$ ft-lb/rad, $K_{o2} = 1.31 \times 10^4$ ft-lb/rad, and $K_{ol} = 3.3 \times 10^4$ ft-lb/rad.

References

[1] Maunder, L., "Natural Frequencies of a Free Gyroscope Supported in Gimbals on an Elastic Shaft," *Journal Mechanic Engineering Science*, Vol. 3, July 1961, pp. 318-323.

[2] Kalley, J.J., Jr. and Mork, H.L., "Development and Air Bearing Test of a Double Gimballed Momentum Wheel Attitude Control System," AIAA Paper 74-488, Los Angeles, Calif., April 1974; also *AIAA Progress in Astronautics and Aeronautics*, to be published.

[3] Briggs, R.W., "Stability of a Two-Degree-of-Freedom Gyro with External Feedback," *IEEE Transactions on Automatic Control*, Vol. AC-10, July 1965, pp. 244-249.